

CHAPTER 1

AN INTRODUCTION TO COMPLEX METALLIC ALLOYS AND TO THE CMA NETWORK OF EXCELLENCE

Jean-Marie Dubois

*Institut Jean Lamour (FR 2797 CNRS-INPL-UHP), Nancy Université,
Ecole des Mines, Parc de Saurupt, Nancy, F-5404
E-mail: jean-marie.dubois@mines.inpl-nancy.fr*

Now that new tools are available to solve the crystallographic structure of complex compounds in metallic alloy systems, a vivid interest manifests itself to discover new compounds in multi-constituent alloys. Several are yet known to contain hundreds or more atoms per unit cell. In the meantime, real efforts are made for better understanding of the properties of these compounds and the mechanisms that underpin the progressive loss of metallic character when the size of the unit cell increases. This introductory chapter focuses at a few examples of this atypical behavior of complex metallic alloys, including quasicrystals as the ultimate state of structural complexity in a crystal made of metals. Examples are transport properties, surface electronic structure, surface energy, wetting and friction. All examples show the same trend, namely apparent localization of electronic states, loss of conductivity, opening of gaps, softening with no work hardening, etc. All phenomena are reminiscent of what is observed in nanostructured metals, but together with the increase of the size of the unit cell. This effect is therefore coined “inverse nanostructuration” by the author who argues that complex metallic alloys help us revisit ancient problems in metal physics, while in parallel potential applications may be sorted out.

1. Introduction

This introductory chapter aims at a short overview of the crystallographic peculiarities and physical properties of Complex Metallic Alloys (CMAs hereafter). Most of the experimental data presented here was obtained quite some time ago and has provided the basis that was used by K. Urban, L. Schlapbach and the author to file an application within the 6th

Framework Program of the European Communities for granting a so-called Network of Excellence (NoE). This successful application came into force in July 2005 and allowed financing the first session of the European School in Materials Science of the *CMA* NoE¹ to which the present book is associated. The focus of the 2006 school was on general aspects of phase transitions in materials, and more specifically on our current knowledge of the transformations taking place in CMAs, from their synthesis to their possible applications. Other sessions will be organized in the coming years, with emphasis on more specific aspects of CMAs. The chapters that follow in this book will give an impressive account of the great progress that was achieved in recent years on CMAs, and also of the many questions that remain only partially solved, or fully open.

CMAs are crystalline compounds of the family of intermetallics that are characterized by a) large unit cells, containing up to thousands atoms, b) the occurrence of well-defined clusters, most often of icosahedral symmetry and c) some disorder, essentially due to the fact that icosahedra do not fill Euclidian 3-dimensional space. Therefore, quasicrystals belong to the family of CMAs, but clathrates also do so.

The properties of CMAs are surprising, although they cannot be claimed unique¹. In Al-based CMAs, electron transport properties (conductivity, Seebeck coefficient, etc.) are governed by the formation of a pseudo-gap (when not a real gap) in the Al 3p partial density of states at the Fermi energy, which results of a combination of Hume-Rothery scattering of electron waves and sp-d hybridization effects^{2,3}. It turns out that surface properties like surface energy, solid-solid friction or wetting also reflect the depth of the pseudo-gap balanced by the presence of d states at the Fermi energy. As a result, it turns out that the surface energy of highly complex intermetallics is so much smaller than that of the metallic constituents of the alloy⁴ that reduced friction or wetting against polar liquids was for long taken as the best examples of potential applications of CMAs^{1,5}.

^a For simplicity in this chapter, italics represent the *CMA* network, whereas normal capital letters (CMA) are for the complex metallic alloys themselves.

Quite a few more properties show the same trend, namely apparent localization of electronic states, loss of conductivity, opening of gaps, mechanical softening with no work hardening, etc. All phenomena are reminiscent of what is observed in nanostructured metals, but take place with increasing the size of the unit cell. This effect is therefore coined “*inverse nanostructuring*” by the author⁶.

In the end, it was admitted by a sufficiently large number of European scientists that the unexpected properties displayed by the few CMAs known so far are fascinating enough, and of strong enough potential interest for technology, to deserve the creation of a new field dedicated to complexity in metallic alloys⁷. The existence of the field was recognized by the foundation of the NoE labelled according to the same acronym *CMA* and funded by the Commission of the European Communities as briefly described at the end of this chapter.

2. Complexity in reciprocal and real space

2.1. A definition of CMAs

An essential question to address at the beginning of this book is to know what we call a CMA. First, it is a compound, or a phase, or an alloy, essentially made of metals. This does not mean that the alloy is a metal itself, or an alloy characterized by metallic properties, because most often the metallic character of the alloy species has become poor or much weaker than in the pure metal constituents. In scarce cases like Al_2Ru , it has turned to semi-conducting. It simply means that the major part of the constituents belongs to sp or d metals (Al, Ga, Sn, Fe, Ni, Pd, W, Rh, Re, etc.), possibly alloyed with semi-conductors (Ge, Si), chalcogenides (Se) and/or rare earths. In few cases, the situation is reversed: the major constituent is the semi-conductor like in clathrates. Oxides, although some may be structurally very complex, are excluded from the CMA family because they present no metallic behaviour whatsoever (except in few cases at very high temperature). The broad variety of chemical combinations that may be synthesized out of about 80 metals in the periodic table participates to the complexity of the compounds

considered in this book. This also means that the potential for discovering new ternary, quaternary, etc. CMAs is huge.

Second, it is often anticipated that complexity is expressed by a difficulty to describe the crystal lattice arrangement due to the large number of independent atomic positions in the unit cell. In many compounds, such a (weak) definition would be acceptable. However, many CMAs do not require lots of independent positions to be accounted for. Very frequently instead, a distribution of occupancy factors must be considered in order to match the chemical disorder inherent to the compound. This is the case for instance of the superstructures of the β -CsCl –type cubic phase that forms in Al-Cu alloys⁸. The basic unit cell is the 2-atom, body-centred cubic unit cell of parameter 0.29 nm. Depending on the Al/Cu composition ratio, substitution vacancies order in the lattice and increase dramatically the size of the unit cell. The largest superstructure known so far forms at composition $\text{Al}_{36}\text{Cu}_{48}\text{V}_{12}$ (V = vacancy), with a unit cell volume 47.7 larger than that of the conventional β -phase.

The example of the superstructures of the β -cubic phase points out the difficulty to describe accurately complexity in real space due to the need to introduce a function that adequately fits the chemical disorder in the lattice, although atomic positions may be easily accounted for by a simple Bravais lattice like body-centred cubic. It is more relevant to call 'complex' an alloy, or a compound, essentially made of metals as presented above, whose reciprocal space exhibits complexity within the Jones zone. The Jones zone is the Brillouin zone constructed with the most important Fourier components in reciprocal space. For a simple crystal, it fits with the first Brillouin zone. When complexity arises, it corresponds to that zone which is built by taking into account the most intense diffraction peaks. A measure of complexity of the crystal is then supplied by the number of peaks that fall inside the Jones zone or equivalently, by the inverse of the reciprocal distance between the first diffraction peak and the origin of reciprocal space: the most complex CMA in a series presents a diffraction peak that falls at the shortest distance to the origin of reciprocal space. In many Al-based compounds, this is a quasicrystal (with in principle 0 distance of the first diffraction peak from the origin of reciprocal space). As an immediate consequence,

metallic glasses are not considered to belong to the group of CMAs, although it is often observed that metallic glasses of specific composition crystallise in a CMA, because they show no sharp Fourier component in their diffraction pattern. The Jones zone is ill defined by the broad main halo in the diffraction pattern and the pre-peak, when it exists, does not fall that close to the origin of reciprocal space. Their physics however is often very much reminiscent of that of CMAs⁹.

As an example of a typical CMA, Fig. 1 illustrates the case of triclinic $\text{Al}_{11}\text{Mn}_4$ (unit cell parameters $a = 0.5087 \text{ nm}$; $b = 0.8848 \text{ nm}$; $c = 0.5052 \text{ nm}$; $\alpha = 89.72^\circ$; $\beta = 100.54^\circ$; $\gamma = 105.37^\circ$; unit cell volume: 0.215 nm^3). The major diffraction peaks fall in the vicinity of the wavevector $q=30 \text{ nm}^{-1}$ ($q=4\pi \sin \theta/\lambda$ with θ the Bragg angle and λ the wavelength) whereas many other peaks of variable intensity are observed inside the range $[0, q]$. The average distance between opposite centres of the facets of the Jones zone is often labelled K_p , so that here we have $K_p \approx 30 \text{ nm}^{-1}$.

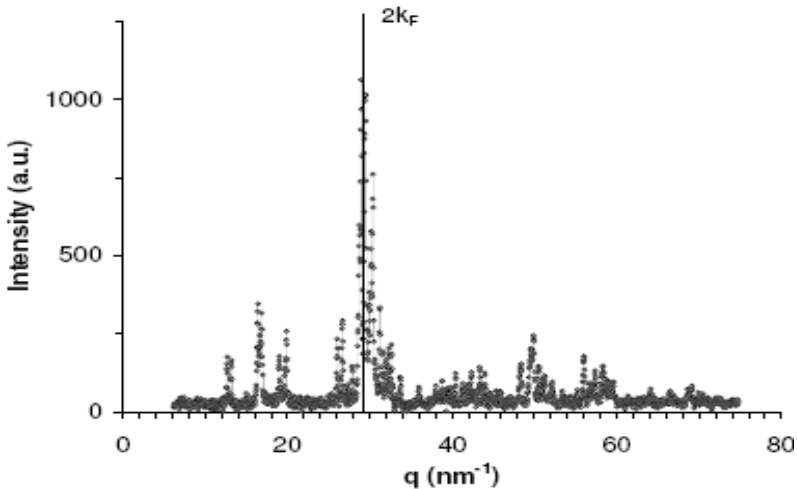


Fig. 1. X-ray diffraction pattern ($\lambda = \text{K}\alpha\text{Mo}$) of triclinic $\text{Al}_{11}\text{Mn}_4$. The x-axis is labelled according to the wave vector q as explained in text. The position of $2k_F$ is shown by a vertical bar, assuming valences of +3 for Al and -3 for Mn. (Courtesy of Dr M. Feuerbacher, CMA).

The number of peaks in the vicinity of $q=1/2 K_p$ reflects the degree of symmetry of the Jones zone. The larger the symmetry of the Jones zone,

the closer the shape will be from a sphere. Such a resemblance to a sphere is actually achieved in many CMAs, for instance, quasicrystals but also γ -brass phases, etc. Furthermore, electronic concentration is very often naturally selected so that a close matching between Jones zone and Fermi surface is observed, which fulfils the Bragg condition $K_P = 2k_F$ (where k_F is the Fermi vector). Such a selection is responsible for the opening of Hume-Rothery gaps and therefore for the enhanced stability of the compound. In $Al_{11}Mn_4$, the Fermi vector amounts to $k_F = 14.25 \text{ nm}^{-1}$ if the contribution to the valence band by Al is taken equal to +3 electrons and that of Mn is assumed negative like in many other transition metals such as Fe, Ru, Re (but not Cu or Pd, see ref. 1 for more information on this point) and equal to -3 electrons according to its position in the periodic table along the 3d-metal series. Hence, it is observed that $2k_F \approx K_P$, a result which is indeed traditionally associated with the formation of a CMA in a given system.

2.2. The example of Al-Cr(-Cu)-Fe alloys

After the pioneer contributions of Pauling¹⁰ and his successors, the Shoemakers, Samson and others, very little was published on Al-based CMAs until the discovery of quasicrystals re-launched the interest for such crystals. Driven by the need to find a quasicrystalline or approximant material offering high corrosion resistance against acids, we considered addition of Cr to Al-Cu-Fe icosahedral crystals^{5, 11}. Above a small concentration in Cr species, the icosahedral phase is no longer stable and is replaced, depending on the Cu/(Cr+Fe) ratio, by orthorhombic or monoclinic compounds of large to very large unit cell. The same trend is observed in Al-Cr-Fe alloys, in which the icosahedral phase is metastable and can be formed only by rapid cooling of the melt¹². Space is too limited here to give a brief description of all compounds discovered in Al-Cu-Fe-Cr alloys (for more details, see ref.1). In the following, I shall concentrate on one single compound, namely the O1-orthorhombic compound of lattice parameters $a = 3.25 \text{ nm}$, $b = 1.22 \text{ nm}$, $c = 2.37 \text{ nm}$, which contains 600 atoms per unit cell (117 independent atomic positions¹³) and has a hierarchical structural

relationship with the more simple rhombohedral γ -AlCrFe brass-type phase¹².

A sketch of the structure is shown in Fig. 2. It consists of a stacking of planar and puckered layers (top left side of the figure).

A projection of the planar and puckered layers, respectively, is shown in the bottom part of the figure. Using pentagonal and flattened hexagonal units, a tiling that although periodic is closely related to a Penrose tiling, is superimposed on the drawing. Close examination of the atom positions reveals the constitutive icosahedral units (Fig. 3) and a large amount of close-packed atomic planes that are interspaced by a distance of 0.43 nm. Such planes were shown by Mizutani³ to play the most important role in transport properties of CMAs because they establish a resonance by propagating electron waves with a Fermi wavelength of $\lambda_F = 0.43$ nm whereas the major Fourier lattice components are located at $K_p \approx 28 - 30 \text{ nm}^{-1}$ in reciprocal space (i.e. $K_p/2 \approx 2\pi/\lambda_F$). The very same situation is observed in the previous example of orthorhombic O1-AlCuFeCr (Fig. 3).

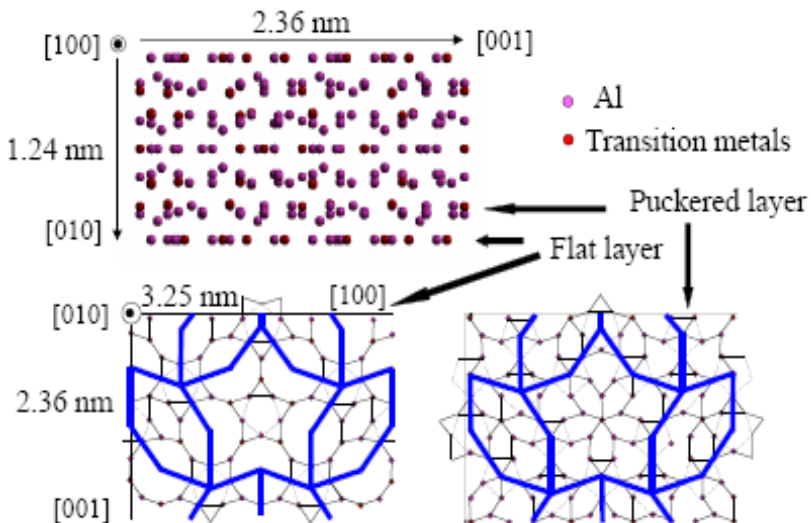


Fig. 2. Sketch of the orthorhombic O1-AlCuFeCr atom structure. The stacking structure of flat (bottom left) and puckered (bottom right) atom layers is shown in the top left part of the structure. Flat layers are very close to perfect pentagonal tiling. (Courtesy V. Demange, *CMA*).

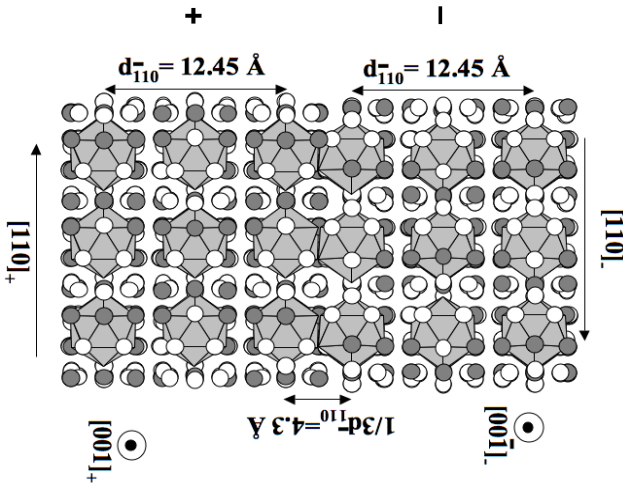


Fig. 3. Formation of icosahedral clusters in O1-AlCuFeCr and their arrangement that shows spacing by 0.43 nm. (Courtesy V. Demange, CMA).

3. The essential property of CMAs

3.1. The pseudo-gap at the Fermi energy

This section is for Al-based CMAs and more specifically for the partial density of states (DOS) of aluminum that may be investigated by a large number of techniques, but preferably in the context of the present chapter by emission (XES) and absorption (XAS) X-ray spectroscopies (see 1 and 2 and references therein).

As just mentioned above, so-called Hume-Rothery (HR) compounds (i.e. compounds for which it is observed that $2k_F \approx K_P$) are electronically stabilized. We shall restrict ourselves to such compounds in this section and the followings. The stabilization mechanism induces a depletion at the Fermi energy (E_F) in the DOS, the so-called Hume-Rothery pseudo-gap¹⁴. Using the XES and XAS techniques, a series of Al-Cu(-Fe) HR compounds of different atomic structures and accordingly different Jones zones were studied in order to investigate the HR pseudo-gap. The valence band (VB) of all these compounds was analyzed together with the Al p and Cu d (-Fe d) conduction bands. In γ -Al₃₅Cu₆₅ as well as in

all Al-Cu(-Fe) samples, the Al $3s-d$ and Al $3p$ sub-bands split in two distinct parts located on each side of the maximum of the Cu $3d$ distributions, around 4 eV¹⁵. Accordingly, the shapes of the Al $3s-d$ and Al $3p$ distribution curves depart dramatically from that in pure Al, which is a typical parabolic curve distorted by experimental artifacts and experimentally induced many-body effects (not shown here, see reference²). This result emphasizes that the free-electron model is no longer valid for HR alloys.

The interaction of Cu with Al can be interpreted within the framework of a Fano-like interaction between highly localized states and extended states¹⁶. The fact that here, the Al partial spectral curves both display a marked depletion exactly at the energy of the maximum of the localized states points out that Al states still retain an extended-like character in these compounds. Using the same methodology as for the HR alloys, we have analyzed several CMAs of much larger unit cells than HR compounds, including icosahedral (i-) and approximants crystals (especially from Al-Cu-Fe system). Again, like in β -Al₅₅Cu₃₃Fe₁₂, it was observed that the valence band of Al-Cu-Fe samples shows that Fe $3d$ states overlap the Al sub-bands edges nearby E_F , Cu $3d$ states are found about 4 eV below E_F , whereas the Al sub-bands overlap each other over the whole extent of the VB, namely over about 12 eV.

In all these samples, it was observed that the intensity of the Al sub-bands at E_F departs from its value in fcc Al. It is lower compared to the pure metal, so that the corresponding valence edges have no longer their half-maximum intensity set at E_F . This more or less pronounced depletion that appears in the Al DOS at E_F , points out the formation of a pseudo-gap. We refer now mainly to Al $3p$ states because (a) in pure fcc aluminum, these states are originally of extended-like character and therefore are more sensitive to changes of the electronic interactions than d states, (b) they are obtained alone by XES whereas this technique gives always d and s states together. To quantify the pseudo-gap of the Al $3p$ partial DOS, we shall restrict ourselves to using only the intensity at E_F , labelled $n(E_F)$ hereafter. It is expressed in arbitrary units, with a value $n(E_F) = 0.5$ in the pure metal, since the inflexion point of the DOS is by

definition located at E_F and at half-maximum in a free-electron system. A summary of a large number of numerical data for $n(E_F)$ is given in Fig. 4.

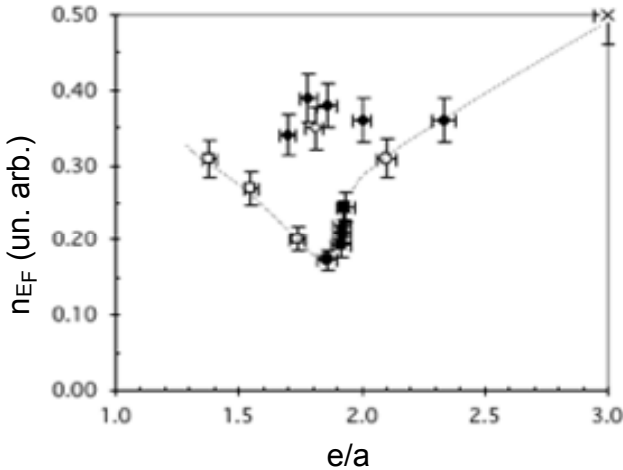


Fig. 4. Variation of the partial $Al3p$ DOS at the Fermi energy $n(E_F)$ as a function of the electron-to-atom (e/a) ratio in Al-Cu-Fe intermetallics¹. The DOS is expressed in arbitrary units: 0.5 stands for pure, fcc Al (cross at the right upper corner of the figure). The diamonds in the middle of the figure are for Al-Cu compounds, open squares for B2, CsCl-type β -cubic phases, the open circle for tetragonal ω - $Al_{70}Cu_{20}Fe_{10}$. The black symbols at the bottom of the curve (which serves only to guide the eye) are for the icosahedral $Al_{62}Cu_{25}Fe_{13}$ compound and its approximants. Observe that there is no real difference of $n(E_F)$ for a quasicrystal and for its closely related crystalline approximants of large unit cell and nearly identical electron concentration. In contrast, the difference is much more marked with respect to smaller crystal unit cells, yet also at identical electron concentration.

Figure 4 demonstrates that the minimum of $n(E_F)$ is obtained for quasicrystals with i) a lattice of very high perfection and b) containing a transition metal (TM) of the mid-series, preferably a $5d$ TM alloyed to a TM of the right hand side of the series like Cu or Pd. However, clearly enough, the minimum of $n(E_F)$ cannot be taken as a unique property because CMAs of very large unit cell and nearly identical chemical composition exhibit almost identical values of $n(E_F)$. This conclusion holds true for all CMAs known so far: physical properties vary in inverse proportion to the size of the unit cell and undergo an extreme at the ultimate size of the unit cell, but no gap is observed when the size of the

unit cell approaches its maximum, for instance infinite size like in an icosahedral quasicrystal.

Actually, a pseudo-gap is expected in most CMAs due to the Hume-Rothery effect, i.e. the interaction of the Fermi Surface with the Jones zone, an effect which in turn stabilizes the crystal structure of the compound. Therefore, the more complex the compound, in other words the closer to a sphere the Jones zone, the more efficient the HR effect and henceforth the deeper the pseudo-gap. The formation of a pseudo-gap was very carefully studied by Mizutani in a large number of γ -brass compounds having 52 atoms in the unit cell³. This work clearly established the origin of the HR mechanism and assigned it to a resonance between Fermi electrons and certain Bragg planes spaced by about 4 nm. The number of such planes may vary, depending on the details of each crystal lattice.

However, hybridization effects between sp and d states deepen and broaden the pseudo-gap more efficiently than the HR effect. This argument was demonstrated both by computations¹⁷ and experimental studies of compounds like Al_2Ru ¹⁸, which as a matter of fact shows the opening of a true, tiny gap of 0.17eV at Fermi energy. Much broader gaps are expected in CMAs containing $5d$ TM elements, but so far none was synthesized¹⁹.

3.2. Transport properties

Space is too limited in this introductory chapter to comment all properties measured so far in CMAs. The reader should refer to reference 1 and to the present book for a state of the art regarding transport properties of CMAs. Experimental determinations of optical conductivity, thermal conductivity, thermo-electric parameters like the Seebeck coefficient were achieved in a rather systematic way for most CMAs known so far and contrasted to theoretical analysis, especially by Macia et al.²⁰.

For the sake of illustration, a blend of several resistivity measurements between liquid helium and room temperature is presented in Fig. 5 for several Al-based CMAs²¹. Surprisingly enough, the low temperature resistivity of those samples varies inversely to the unit cell

size and presents a change of the sign of the temperature coefficient of resistivity (TCR) when the unit cell becomes large, with remarkably a zero-TCR at a specific composition (and crystal structure).

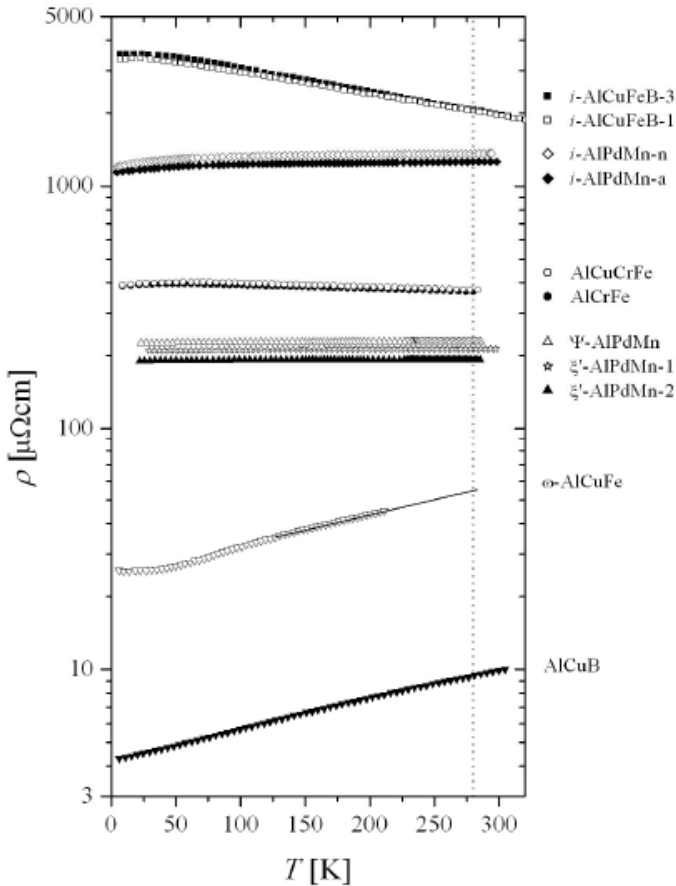


Fig. 5. Electronic resistivity of a variety of CMAs with different unit cell sizes²¹. Icosahedral CMAs are located in the upper part of the figure, O1-orthorhombic compounds are labelled O-AlCrFe and O-AlCuCrFe whereas a large unit cell AIPdMn CMA and its superstructures²², noted Ψ and ξ' , respectively, fall in the middle of the figure with a zero TCR. The notation ω -AlCuFe is for the tetragonal ω -Al₇Cu₂Fe compound and AlCuB is for a superstructure of the AlCu β -phase⁸ doped with 1 at% of boron. Observe the TCR, which marks the transition from normal metallic behaviour (small unit cell size) to an unexpected behaviour for a system made of metals (large unit cells).

This observation has triggered a large research effort to understand better the transition from usual metallic behavior (small unit cell size) to a behavior much more resembling that of a semi-conductor. In the first regime, the diffusion of charge carriers follows a ballistic law, i.e. is proportional to time t and Einstein's conductivity applies in proportion to $N(E_F)$, the total DOS at E_F . In the second regime, conductivity is instead proportional to $[N(E_F)]^2$ and diffusion follows a t^β regime, with $0 \leq \beta \leq 1$ ²³. Essentially, it was concluded that the breakdown of Bloch's theorem at large to infinite unit cell size is accompanied by the formation of so-called critical states, neither extended, nor fully localized like in a totally disordered medium²⁴. Further analysis by Mizutani³ and others^{25, 26} has concluded to a transport mechanism by hopping in highly complex CMAs such as quasicrystals and their approximants, in total contrast to the usual behavior of alloys.

3.3. Mechanical properties

The study of large unit cell CMAs and of quasicrystals under compression stress at high temperature was for some time hesitating, concluding first that plasticity was carried by glide of dislocations and later by climb. Finally, climb assisted by phason jumps appeared to be the most important mechanism for icosahedral quasicrystals²⁷, but a general view at all possible deformation mechanisms of CMAs remains still to be worked out. A mechanism specific to large unit cell CMAs, called metadislocation, was discovered to be able to generate plasticity on the basis of very local rearrangements of structural units²⁸.

The situation is quite similar as far as contact mechanical properties (at much lower temperatures) are concerned, although it was recognized soon after the discovery of quasicrystals that friction is significantly reduced against metallic antagonists like steel²⁹. A fairly illustrative example of the contrast to be expected regarding friction between a normal metallic crystal and an aperiodic CMA riding against a steel antagonist is provided by Fig. 6. It shows the data recorded during a pin-on-disk experiment performed at a low residual pressure (typically 10^{-5} mbar) and a velocity of the disk relative to the pin of $5 \cdot 10^{-4}$ m s⁻¹. These parameters were chosen in such a way that a full layer of oxide has no

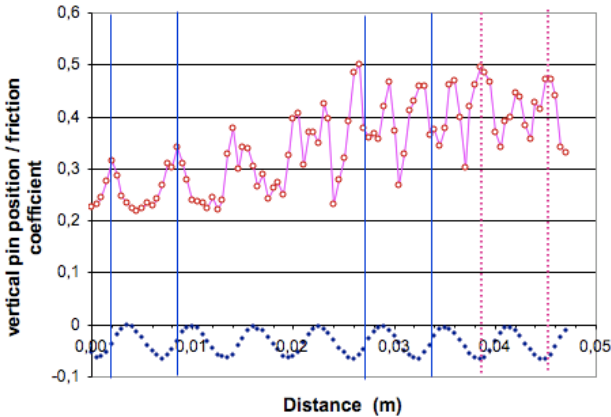


Fig. 6. Pin-on-disk experiment in vacuum ($1.9 \cdot 10^{-6}$ mbar), using a hard Cr-steel ball of 6 mm diameter riding under a normal load of 1N on a mono-domain Al-Ni-Co decagonal single crystal at a linear velocity of $5 \cdot 10^{-4}$ ms⁻¹. The upper curve (open dots) is for the friction coefficient μ and the lower curve for the vertical position of the pin (see text). Two successive maxima of this curve mark the length of a full circular trace of the indenter in contact with the surface of the single crystal (diameter of the trace 3 mm). At the beginning of the experiment, the decagonal sample is covered by a thin layer of its native oxide, namely amorphous alumina. Due to a slight misalignment of the specimen surface with respect to a perfectly horizontal position, the maxima of friction coincide with the middle of the ‘up-hill’ part of the trace (solid vertical bars). Therefore, right after the test has started, friction on the amorphous oxide is isotropic as expected in the sample surface plane. The oxide layer is removed after two turns of contact with the indenter and friction switches to another regime. New peaks appear, superimposed on the ones due to horizontal misalignment. More specifically, two maxima (respectively, minima) of friction show up during one single rotation (dashed vertical bars), which clearly fits with half the previous period. Careful examination of the angular position of the single crystal on the disk holder proves that the maxima of friction coincide with the pin riding along the periodic stacking direction in the crystal whereas the minima are observed when the rider moves perpendicular to this direction.

time to grow in the time interval left between two successive passages of the indenter on the disk. Immediately after the beginning of the test, the native surface oxide inherited from exposure to ambient atmosphere of the sample is broken through by the pin. In Fig. 6, this operation takes two turns of the disk (about 0.012 m). After this point, the two naked pin and disk surfaces come into contact.

The data shown in Fig. 6 was obtained using a single grain of the Al-Ni-Co decagonal phase, a material characterized by periodicity along one

direction, and loss of periodicity perpendicularly to this direction. The stacking period is about 0.4 nm. Therefore, it is possible to probe the respective effects of periodicity and aperiodicity using the very same sample. The key point is that a large difference of the friction coefficient $\mu = F_T/F_N$ is observed depending on whether friction occurs along the periodic stacking direction of the single crystal or perpendicular to it (F_T represents the tangential force that works against the movement of the pin, and F_N is the normal load applied to the pin, here 1N). In other words, the measurement of the tangential force F_T (Fig. 6) leads to a friction coefficient $\mu = F_T/F_N$ that returns to the same value with a period equal to the length of one turn (or a time periodicity equal to the duration of one rotation) when the test starts whereas it shows half that periodicity when pin and decagonal sample come in contact (beyond 0.012 m riding distance). This means that friction on the amorphous native oxide is isotropic (the slight variation of μ when one rotation proceeds is due to a misalignment of the sample surface against a perfectly horizontal plane, which causes friction forces when the pin goes 'down-hill' and 'up-hill' to be different (the vertical position of the pin is also shown in figure 6, which in turn supplies us with a reference for the position of the pin along the circular trace). After two turns, the oxide layers are broken and the pin comes into contact with the naked surface of the specimen. Then, it appears that the period of μ is no longer that of one full rotation, but only half a turn. Within one rotation, two peaks of μ are now visible, one of rather large amplitude, going from $\mu = 0.25-0.30$ at its minimum up to $\mu = 0.5$ at its maximum whereas the other peak exhibits intermediate values of μ . This situation remains unchanged for quite a significant number of pin-on-disk turns, until wear debris and severe plastic deformation of the surfaces in contact disturb the quality of the experiment.

The simple example above illustrates the variety of friction conditions experienced on CMAs, but so far, the example of the decagonal phase is unique as was first pointed out by Park et al.³⁰. Many more data was collected by the author, especially on Al-based binary CMAs^{1, 31}. In the coming section, the main contribution to friction in vacuum is assigned to the (reduced) adhesion properties of Al-based CMAs and therefore to the (lower) surface energy of these materials.

These results have direct relevance to technological applications, especially hindrance of cold welding in aerospace mechanisms or cutting tools.

3.4. Chemical properties

At least for Al-based CMAs, chemical properties are disappointingly determined by the constituents introduced in the complex alloys: the presence of elements like Cr or Mo enhances corrosion resistance, especially when pitting corrosion occurs^{1,32}, oxidation resistance is pretty good, including up to temperatures far above room temperature (e.g. 700-900 K for alloys that melt in the range 1200-1500 K) thanks to the passivating role of aluminum dioxide that is well documented in conventional alloys of this element¹, etc.

Two different chemical properties that benefit from complexity of the CMA lattice have been pointed however. The first is the catalytic efficiency of nano-domains of Cu or Pd prepared by etching a quasicrystal in an alkaline solution³³. The beneficial effect results from a combination of properties. On the one hand, pure metal nanograins of the late transition metal (Cu or Pd) may be grown out the surface of the powdered CMA by etching and releasing it in a mixture of amorphous oxides of the other elements (i.e. Al and Fe or Mn, respectively). On the other hand, coarsening of the grains is prevented by the presence of the second TM, with which the enthalpy of mixing is negative. As a consequence, the catalytic activity of this type of material, used for instance for methanol reforming, is at least equal, if not superior to that of the pure, ultra-divided metal whereas savings are achieved on the quantity of catalyst and its preparation processing.

Another challenging chemical property is hydrogen storage, which raises great interest in our community, see the program of the second CMA EuroSchool that is going to take place in May 2007³⁴. The hydrogen capacity of Ti-Zr-Ni icosahedral compounds, to a lesser extent their crystalline approximant, reaches a H/M atom ratio of 2 (H: number of stored hydrogen atoms; M: total number of Ti, Zr and Ni atoms)³⁵. This represents a considerable amount of hydrogen that is comparable or even superior to the performance of more conventional metal hydrides.

The key point is that a very large number of tetrahedral sites form in the lattice, in relation to the complexity of the icosahedral structure, which are favorable sites to insert a H atom. Furthermore, the chemical composition yields TM atoms (e.g. Zr) that preferably bond to H atoms and are sitting on one or two vertices of these tetrahedral sites.

However, technological difficulties are still there, such as an insufficiently long lifetime, or equivalently a too small number of load/unload cycles that are required for a commercial battery, which so far did not open the way to the usage of this type of CMAs in commercial devices. Furthermore, lighter materials such as Mg look more promising in respect of the H/M weight ratio. This is also a good reason to pursue a research on Mg-based CMAs, again trying to combine atom compositions with a large affinity for H and the presence of the largest possible number of tetrahedral traps for H atoms.

4. Surface energy

4.1. Surface energy in general

As far as Al-based CMAs are concerned, surface energy (noted γ_s in the following) combines chemical physics with contact mechanical properties as we try to demonstrate in this section. It is a very important property which determines the cleavage energy of a solid, the equilibrium shape of a crystal, the wetting properties of both solids and liquids, the nucleation rate of a second phase (via the energy born at the interface), etc. It is however very difficult to assess experimentally, either by contact angle measurements or flow stress measurements at the approach of the melting point because of the need to employ single crystals with no defects emerging at the surface. Indirect assessment of the surface energy may be based on contact angle measurements of liquids wetting the surface of interest, but this also is a very difficult task for experimental reasons (contamination of the surfaces, high temperatures, etc.) and because the energy of the interface between solid and liquid is most often ignored³⁶. In the case of CMAs, the number of different samples and the difficulty to grow them all as mono-domain samples simply rules out this route. Computer physics is more efficient

to calculate the surface energy of metals and simple alloys and was successfully applied to a large number of metals and pure elements³⁷. Due to the limited power of computers, it is at present days limited to a small number of atoms per unit cell and cannot be applied to CMAs and even more so to quasicrystals.

The importance of friction and wetting in potential applications of CMAs, and furthermore the need for a better understanding of the fundamentals that govern those properties, forced us to find a simpler method to assess approximately γ_s for a large number of CMAs of various compositions. This method, although far less accurate than the ones evocated above, is described in the following.

4.2. Experimental

Placed in a vacuum chamber evacuated down to 10^{-6} mbar or less, a pin-on-disk instrument allows us to measure the friction coefficient between a hard steel ball and the solid of interest without intervening artifacts like moisture or external contamination (refer to previous section). Tribo-oxidation however may play an important role as was noticed elsewhere for tests in ambient atmosphere³⁸. This artifact is dramatically reduced if the relative velocity of the indenter to the disk is large enough to forbid the growth of a full oxide layer in the time interval elapsed between two successive passages of the indenter, whereas the native oxide always present at the surface of our samples is broken and disappears from the trace within very few passages at the beginning of the experiment. This experimental procedure was applied in a systematic way to a large number of samples prepared by sintering according to a standard procedure depicted in ref.¹. After polishing these samples (diameter 20 mm, thickness 4-6 mm) down to mirror polish, the specimens were placed in a pin-on-disk set up housed in a vacuum chamber as explained already in the previous section. The friction coefficient μ was recorded continuously during each test, using the same parameters as given in the previous section. Careful examination of the contact trace was performed after each test, for both the steel ball indenter and the surface of interest, thus allowing an evaluation of the wear produced during the test. In most cases, but not all, wear appeared negligible.

Theoretical models were developed to understand better the origin of Admontons law $F_T = \mu F_N^{39}$. Some of them take adhesion forces explicitly into account, but unfortunately require some information that is missing in our experiments (e.g. the actual contact area). As a much easier to handle test model, we shall assume that:

$$\mu = \alpha/H_V + \beta \Omega_{SP} \quad (1)$$

where the material (Vickers) hardness is noted H_V , the work of adhesion (under these specific experimental conditions) of the steel pin P on the surface S is Ω_{SP} and α and β represent calibration parameters which may be determined easily by producing the same experiment, but for a series a materials of known hardness and surface energy as explained in reference 40. Since wear is most often negligible, we furthermore assume that Ω_{SP} is actually the reversible adhesion energy of P onto S: $\Omega_{SP} = \gamma_S + \gamma_P - \gamma_{SP}$ with γ_P the surface energy of the pin and γ_{SP} the interfacial energy at equilibrium between S and P materials. This is obviously a very drastic assumption that can only be marginally valid for a pin-on-disk test, but it is strengthened by the very slow motion of the pin relative to the CMA solid and the (near) absence of wear. On top of this, we take $\gamma_P - \gamma_{SP} = 0$, which means that we overestimate the value of γ_S that can be obtained after inverting Eq. 1, or:

$$\gamma_S \leq (\mu - \alpha/H_V)/\beta \quad (2)$$

Calibration of Eq. 1 using known materials (metals, alloys, oxides) leads to a linear fit characterized by a regression coefficient very close to 1⁴⁰, which makes us very confident in the validity of the method. Yet, it must be insisted on the fact that instead of measuring γ_S , we just supply an estimate of its upper limit for a large number of the CMAs of interest here.

4.3. Data analysis and upper limit of γ_S

Table 1 and Fig. 7 summarize our findings regarding the estimation of the surface energy of Al-TM CMAs (in this sub-section, TM represents one or two 3d metals).

Table 1. Pin on disk tests in vacuum on Al-based CMAs of varying composition and crystal structure: experimental results and estimated values of γ_s .

Compound (at.% or atoms)	Crystal structure	Vickers Hardness (load 0.5 N) $\pm 8\%$	Friction coefficient $\pm 15\%$	Estimated γ_s (Jm ⁻²) $\pm 25\%$
Al ₃ Ti	tetragonal	604	0.6	1.72
AlTi	B2-cubic	277	0.7	1.86
Al ₃ V	tetragonal	427	0.7	1.97
Al ₉ Cr ₄	γ -brass	695	0.48	1.37
Al ₈ Cr ₅	γ -brass	720	0.49	1.40
Al ₁₁ Mn ₄	triclinic	476	0.41	1.09
β -AlCo	B2-cubic	620	0.5	1.41
l-Al ₁₃ Co ₄	monoclinic	700-800	0.75-0.8	2.2 – 2.4
β -AlFe	B2-cubic	417	0.64	1.78
λ -Al ₁₃ Fe ₄	monoclinic	815	0.69	2.0 ₄
Al ₃ Ni	orthorhombic	662	0.45	1.27
Al ₂ Cu	tetragonal	550	0.44	1.21
γ -Al ₉ Cu ₄	cubic	480	0.37	1.0
AlCu	hexagonal	806	0.3	0.82
oF-Al ₃ Cu ₄	orthorhombic	710	0.24	0.6 ₂
ϕ -Al ₁₀ Cu ₁₀ Fe	cubic	650	0.32	0.9
β -Al ₅₅ Cu ₃₀ Fe ₁₅	B2-cubic	680	0.31	0.8 ₄
ω -Al ₇₀ Cu ₂₀ Fe ₁₀	tetragonal	640-640	0.6-0.75	1.7-2.0
Al ₆₂ Cu _{25.5} Fe _{12.5}	icosahedral	780	0.26	0.5 ₅
Al ₅₉ B ₃ Cu _{25.5} Fe _{12.5}	icosahedral	790	0.21	0.5 ₄
Al ₇₀ Pd ₂₀ Mn ₁₀	icosahedral	750	0.3	0.8 ₂

First, one should notice that some CMAs, especially quasicrystals (large diamond symbols in Fig. 7) exhibit a particularly low surface energy compared to that of the constituent $3d$ metals (typically 2.2 J/m² for Fe) and that of Al (1.15 J/m²) as well as to conventional binary intermetallics (for example, triangles in Fig. 7). Worth mentioning, Al-Cu binary compounds (squares in Fig. 7) are also characterised by a rather low surface energy. Second, the surface energy follows a smooth decrease with the filling-in of the valence band.

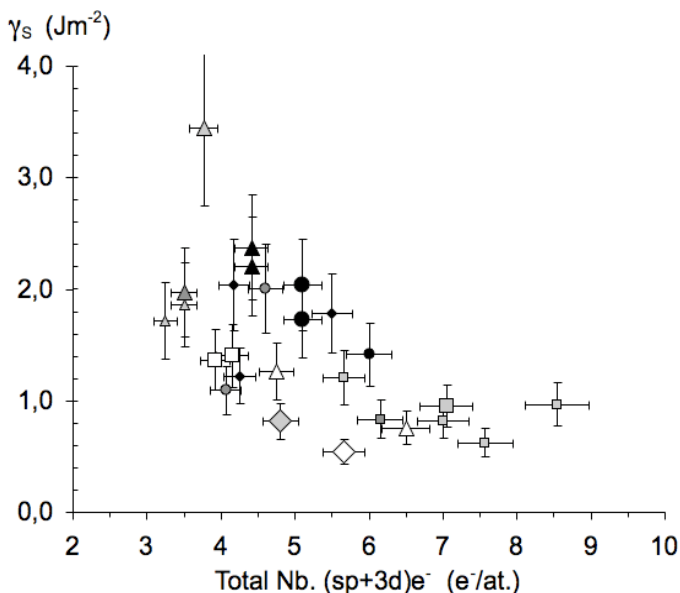


Fig. 7. Variation of γ_s with the total number of s, p and 3d electrons in the molecular composition of Al-3d TM CMA samples. Large open and grey diamonds stand for i-AlCuFe and i-AlPdMn compounds, respectively. Grey squares represent Al-Cu, open triangles Al-Ni, grey triangles Al-V (large symbol) and Al-Ti (small symbol), open squares Al-Cr, grey dots Al-Mn, small solid diamond Al-Fe CMAs, respectively. Black solid triangles and black solid dots are for $\text{Al}_{13}\text{Co}_4$ and $\omega\text{-Al}_7\text{Cu}_2\text{Fe}$ compounds (two separate measurements on two distinct samples each), respectively. The top grey triangle is for Al_8V_5 , but this estimate is rather uncertain due to the contribution of wear to friction.

Scrutinizing Fig. 7 shows that γ_s is smaller for TM alloying elements that belong to the right hand side of the 3d series whereas elements like V, Ti, Mn, Co or Cr are associated with much larger values of γ_s (grey and black symbols in Fig. 7). Nevertheless, quasicrystals are located significantly below average at a given electron concentration, an effect most presumably related to the formation of critical states and their unusual contribution to the valence band at the Fermi energy. Similarly, large differences in γ_s are observed for compounds of comparable chemical composition, but different TM content. This is the case for instance for β - and γ - compounds of the Al-Co and Al-Fe systems (Table 1). The two types of compounds are characterized by

values of γ_S that differ by a factor of nearly 2, a difference that must be related to the HR pseudo-gap existing at E_F and to the respective abundance of s , p and d states in the surface electronic structure (see also Fig. 4). More work is in progress to understand better the possible role of the pseudo-gap in determining γ_S .

5. Inverse Nano-Structuration

5.1. Comparison to Conventional Nano-Structuration

To sum up at this stage of the chapter, I shall remind the Reader that both the Hume-Rothery scattering of Fermi electrons and $sp-d$ hybridization contribute to the formation of a deep pseudo-gap at Fermi energy in large unit cell CMAs. In few compounds, a true gap is open. The width and depth of the pseudo-gap are in proportion to the size of the unit cell (although no analytical exact expression that would account for the coupling has been worked out till now). A change of behavior of the transport properties is observed from normal metallic transport to a hopping mechanism when the size of the unit cell becomes comparable to the Fermi wavelength, i.e. when the lattice parameters reach approximately 1 nm or more. Associated with this fundamental characteristic of CMAs are numerous other effects that could not be introduced in the present chapter for the sake of brevity, but are illustrated elsewhere in this book and in review documents quoted in¹. For the same range of lattice parameters, plasticity becomes one more essential property of CMAs and is carried by defects intrinsic to the lattice complexity of CMAs²⁷. Specific chemical reactivity is not associated with the size of the unit cell of CMAs, although after etching it becomes quite clear that catalytic performance is only observed with Al-Cu-Fe CMAs of large unit cell, and not with more simple materials like the ω -Al₇Cu₂Fe phase.

Altogether, such effects are considered a specific behavior of nanostructured materials, in association with the reduction of the size of constitutive (isolated) objects, or with the relatively higher importance of interfaces and surfaces compared to the volume of a bulk specimen synthesized from nanograined material. The comparison is made for

illustration in Fig. 8 between plasticity under compressive stress of nanograined ultra-pure copper⁴¹ and an Al-Cu-Fe-Cr orthorhombic of approximant of the decagonal quasicrystal⁴².

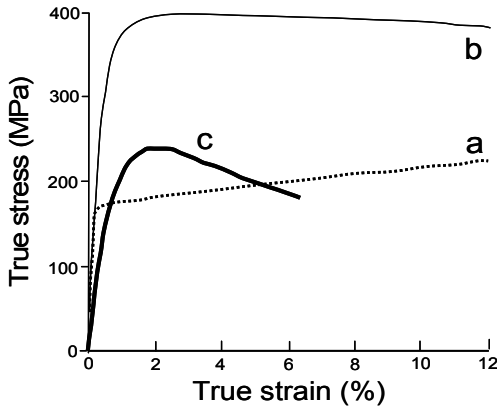


Fig. 8. True stress-true strain curves recorded during compression testing at room temperature of microcrystalline copper (a) and nanocrystalline copper (b) of average grain size 50 nm⁴¹ compared to orthorhombic Al-Cu-Fe-Cr CMA (c) at 650°C⁴². Observe the absence of grain coarsening on curves b) and c).

In the former sample, the average size of the Cu grains is about 50 nm whereas in the latter, the grain size is a fraction of a millimeter. The stress-strain curves are however nearly identical because plastic deformation is due to the collective movement under stress of localized atomic defects, which go with the disorder installed in the respective materials.

The occurrence of localized-like (critical) states, the change. transport regime of conductivity, the plasticity associated with atom jumps, the surface chemical reactivity that raises with increasing the size of the unit cell beyond a significant fraction of a nanometer (typically 1 nm) is coined Inverse Nanostructuration (INS) by the author. It is directly associated with the potential of CMAs for technology, see next section An oversimplified picture of the main effects encountered in conventional nanostructuration, when the size of the individual objects or the grain size in a composite material becomes small (typically below few nanometers), and INS is given in Fig. 9 and its caption.

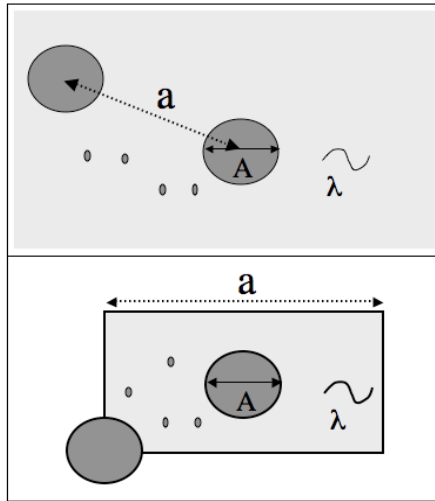


Fig. 9. Simplified comparison between conventional nanostructuring (CNS, top part of the figure) and inverse nanostructuring (INS, bottom part of the figure). In CNS, the parameters that matter are the size A of the objects (large circles) and their respective interspacing distance a compared to the wavelength λ of the excitation. The presence or not of disorder (featured by small dots) between the separate objects, for instance contamination, dust, ill-grown particles, etc. also determines the response of the system to the excitation. The size of the system (e.g. a terrace on a single-grain wafer, light grey area) is supposed infinite, or much larger than the individual size of the objects. Effects of relevance to the small size of the system components manifest themselves when their size becomes small, i.e. when $A \approx \lambda$ whereas the separation distance a cannot be very large in order to observe a coupling between the objects, typically $a \geq \lambda$. In INS, the situation is reversed. The individual objects are the atom clusters (large circles of diameter A) embedded in a periodic crystal having a unit cell of lattice parameter a , which is approximately the separation distance between individual clusters. Here also, there is some disorder between the clusters, often called 'glue atoms' (small dots). Effects due to INS manifest themselves when $A \approx \lambda$, like in CNS, and when $a \geq \lambda$, preferably when $a \gg \lambda$. This supposes that the more complex the compound, equivalently the larger the unit cell, the more enhanced the effects of INS.

5.2. A great potential for future research

Accessible due to very recent progress in materials science, CMAs offer great potential for innovation. Examples of this potential are heat insulation at low temperature (using e.g. Al-Cu-Fe compounds), hydrogen storage, thermoelectricity, enhanced catalytic efficiency at

lower cost, reduced friction, optimised composites, nanostructuring of metallic aggregates or thin films, development of innovative coating processes adapted to complex surface shapes, etc. Thermoelectricity is of special relevance nowadays that green energies are foreseen. Most presumably, clathrates and skutterudites offer the best CMA candidates for this purpose with quite respectable figures of merit achieved so far. Already mentioned, there are some doubts about the actual usefulness of CMAs regarding hydrogen storage in competition with light materials and especially nanotubes, but the challenge is worth a serious research effort. To end with, composite materials containing CMAs are the subject of various attempts for application in view of enhanced mechanical performance, whether they are prepared by blending with polymers or light metals or by in-situ reinforcement produced by nano-precipitation of particles. Thanks to their low surface energy, grain coarsening is prevented, but direct usage of the specific surface energy is also foreseen in order to prevent cold-welding of mechanical parts kept in contact under severe load, for instance in satellites or vacuum technology applications.

6. Goals and organisation of the NoE CMA

On this basis, a European network uniting 20 high-level core institutions in Europe, with a staff of more than 300 scientists and 60 PhD students, was designed to strengthen the competitiveness of European industries wherever materials need to offer *hybrid properties*, being both structural and functional, or embody an extraordinary *combination of properties* that are mutually excluding in conventional materials. Innovative management procedures for knowledge handling and networking, grant administration, organisation of conferences, exhibitions, industrial open days and specific measures for personnel exchange, access to platforms and durable integration of women in science are being taken, together with an ambitious program of summer schools and personnel training.

The main purpose of a European Network of Excellence is to counterbalance the fragmentation of research in the continent. The essential tool used by *CMA* to achieve integration is the creation and functioning of so-called VILs, or Virtual Integrated Laboratories, in

conjunction with VIUs, or Virtual Integrated Units. These latter VIUs are service units that assist the VILs along their scientific strategy and needs (executive board and network office, gender mainstreaming, publications, mission service, transfer of knowledge and innovation, legal expertise). A very important VIU in this respect is the EuroSchool that has produced the present book.

Six VILs were created, which assemble the expertise found in various European countries regarding metallurgy (VIL A), crystallography (VIL B), physical properties (VIL C), surface physics, chemistry and nanosciences (VIL D), surface technologies (VIL E) and finally applied physics of CMAs (VIL F). The degree of integration through the creation and functioning of the VILs can be appreciated from Fig. 10, which for the sake of simplicity presents only partial information on the exchange of data and deliverables between VILs and the external scientific community.

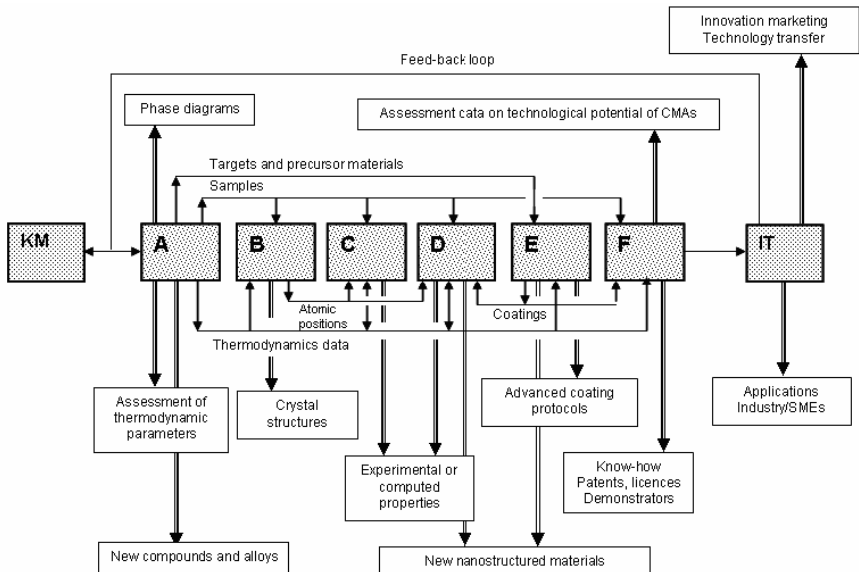


Fig. 10. Virtual Integrated Units of the *CMA* network of excellence, their relationships to each other and to the external world (simplified).

As an example, VIL A will supply the other VILs with well-characterized samples, for structure determination, property measurements or assessment of potential applications (shown by single-line arrows). On the other hand, output of VIL A relevant for the external world such as the discovery of new compounds, phase-diagram data and measured or computed thermodynamic properties, will be distributed via scientific publication (double-line arrows). There is therefore a clear will of CMA to establish integration both within a VIL, binding together various topically related laboratories, and between different VILs in order to forward co-operation between different communities.

Acknowledgments

Thanks are due to the Commission of the European Communities for partial support of my work over the years (Grants BRE 2 CT 92 0171, G5RD-CT-2001-00584 & NMP3-2005-CT-500145). The author also gratefully acknowledges the long-lasting support of his research by the local authorities in Nancy (Communauté Urbaine du Grand Nancy, Conseil Régional de Lorraine and Préfecture de la Région Lorraine). Thanks also go to Dr M. Feuerbacher, Forschungszentrum Juelich, Germany, for the provision of the X-ray data shown in Figure 1 and Prof. P. A. Thiel and her project team at Iowa State University, USA for the provision of the single grain decagonal sample used in part of this work. I am also deeply grateful to M. Sales, J. Brenner and A. Merstallinger, Austrian Research Centres, Seibersdorf, for providing access to the pin-on-disk facility and experimental help.

References

1. J.M. Dubois, *Useful Quasicrystals* (World Scientific, Singapore, 2005).
2. E. Belin-Ferré, *J. Phys. Cond. Matter* **14**, R789 (2002).
3. U. Mizutani, *The Theory of Electrons in Metals*, (Cambridge University Press, Cambridge, 2001); U. Mizutani, in *The Science of Complex Alloy Phases*. Ed. T.B. Massalski and E.A. Turchi (The Minerals, Metals and Materials Society, Warrendale, 2005).
4. J.M. Dubois et al., *Phil. Mag.* **86-6-8**, 797 (2006).

5. J.M. Dubois and A. Pianelli, *French Patent* n° 2671808 (17-06-1994); *US Patent* n° 5432011 (11-07-1995).
6. J.M. Dubois, *Robert F. Mehl Lecture 2007*, (TMS Conf. Proceedings, Warrendale), to be published (2007).
7. For more details, see the website of CMA at: www.cma-ecnoe.org.
8. C. Dong, Q.H. Zhang, D.H. Wang and Y.M. Wang, *Euro Phys. J.* **B 6**, 25 (1998).
9. P. Häussler, J. Barzola-Quiquia, D. Hauschild, J. Rauchhaupt, M. Stiehler and M. Hackert, in *The Science of Complex Alloy Phases*, Ed.. T.B. Massalski and P.E.A. Turchi (The Minerals, Metals and Materials Society, Warrendale), pp.43-86 (2005).
10. L. Pauling, *The Nature of the Chemical Bond*, 3rd Edition, Chap. 11, (Cornell University Press, Cornell, 1960).
11. C. Dong and J.M. Dubois, *J. Mat. Science*, **26**, 1647-1654 (1991).
12. V. Demange, J.S. Wu, V. Brien, F. Machizaud and J.M. Dubois, *Mat. Sc. Eng.* **294-296**, 79-81 (2000).
13. X. Z. Li, C. Dong and J.M. Dubois, *J. Appl. Cryst.* **28**, 96-104 (1995).
14. A.P. Blandin, in *Phase stability in metals and alloys*, Ed. P.S. Rudman, J. Stringer, R.I. Jaffee (McGraw Hill, New York), 115 (1965).
15. V. Fournée, E. Belin-Ferré and J.M. Dubois, *J. Phys.: Cond. Matter* **10**, 4231 (1998).
16. K. Terakura, *J. Phys F: Met. Phys.* **3**, 1773 (1977).
17. G. Trambly de Laissardière, D. Nguyen Manh, L. Magaud, J.P. Julien, F. Cyrot-Lackmann and D. Mayon, *Phys. Rev.* **B 52**, 7920 (1995).
18. D. Nguyen Manh, G. Trambly de Laissardière, J.P. Julien, D. Mayou and F. Cyrot-Lackmann, *Solid State Comm.* **82**, 329 (1992).
19. M. Krajci and J. Hafner, *Mat. Res. Symp. Proc.* **805**, 121 (2004).
20. E. Macia, *Phys. Rev.* **B 66**, 174203 (2002); C.V. Landauro, E. Macia and H. Solbrig, *Phys. Rev.* **B 67**, 184206 (2003).
21. E. Belin-Ferré, M. Klansek, Z. Jaclic, J. Dolinsek, J. M. Dubois. *J. Phys.: Condens. Matter* **17**, 6911 (2005).
22. L. Behara, M. Duneau, H. Klein and M. Audier, *Philos. Mag.* **A 76**, 587 (1997).
23. D. Mayou, in *Quasicrystals, Current Topics*, Ed. E. Belin-Ferré et al. (World Scientific, Singapore, 2000).
24. C. Sire, in *Lectures on Quasicrystals*,. Ed. F. Hippert and D. Gratias (Les Editions de Physique, Les Ulis, 1994).
25. C. Janot, *Quasicrystals, a Primer*, 2nd Edition (Clarendon Press, Oxford, 1994).
26. V. Demange, A. Milandri, M.C. de Weerd, F. Machizaud, G. Jeandel, J.M. Dubois, *Phys. Rev.* **B 65**, 144205 (2002).
27. F. Monpiou, D. Caillard and M. Feuerbacher, *Philos. Mag.*, **84**, 2777 (2004).
28. H. Klein, M. Feuerbacher, P. Shall and K. Urban, *Phys. Rev. Lett.* **82**, 3468 (1999).
29. J.M. Dubois, S.S. Kang, J. von Stebut, *J. Mat. Sc. Lett.*, **10**, 537 (1991).
30. Jeong Young Park, D.F. Ogletree, M. Salmeron, R.A. Ribeiro, P.C. Canfield, C.J. Jenks and P.A. Thiel, *Science* **309**, 1354 (2005).

31. E. Belin-Ferré and J.M. Dubois, *Int. J. Mat. Res.* **97**, 7 (2006).
32. D. Veys, C. Rapin, X. Li, L. Aranda, V. Fournée, J.M. Dubois, *J. Non Cryst. Sol.* **347/1-3**, 1 (2004).
33. A.P. Tsai and M. Yoshimura, *Mat. Res. Soc. Symp. Proc.* **643**, K16.4.1 (2001).
34. See the website of the Euroschool at: <http://euroschool-cma.ijs.si>
35. A.M. Viano, R.M. Stroud, P.C. Gibbons, A.F. McDowell, M.S. Conradi and K.F. Kelton, *Phys. Rev. B* **51-17**, 12026 (1995).
36. N. Eustatopoulos, M.-G. Nicholas and D. Drevet, *Wettability at High Temperatures*, Elsevier, Amsterdam (1999).
37. L. Vitos, A.V. Ruban, H.L. Skriver and J. Kollar, *Surf. Science* **411**, 186 (1998).
38. I.L. Singer, J.M. Dubois, J.M. Soro, D. Rouxel and J. Von Stebut, in *Quasicrystals*, Ed.S. Takeuchi and T. Fujiwara, World Scientific Singapore 769 (1998).
39. Jianping Gao, D.W. Luedtke, D. Gourdon, M. Ruth, J.N. Israelachvili and Uzi Landman, *J. Phys. Chem. B*, **108**, 3410 (2004) and references therein. D. R. Bates, *Phys. Rev.* , 492 (1950).
40. J.M. Dubois, M.C. de Weerd and J. Brenner, *Ferroelectrics* **305**, 159 (2004).
41. Y. Champion, C. Langlois, S. Guérin-Mailly, P. Langlois, J.L. Bonnentien and M.J. Hÿtch, *Science*, **300**, 310 (2003).
42. S.S. Kang and J.M. Dubois, *Philos. Mag.* **A 66-1**, 151 (1992).